Applied Thermal Engineering 123 (2017) 1181–1189

Contents lists available at ScienceDirect

Applied Thermal Engineering

journal homepage: www.elsevier.com/locate/apthermeng

Research Paper

Experimental investigation of heat transfer with ash deposition in ultra-low temperature WHRS of coal-fired power plant

Yuetao Shi [a,*], Chen Dai [a], Zhihao Ma [a], Zhixiong Guo [b,*]

[a] School of Energy and Power Engineering, Shandong University, Jinan, China
[b] Department of Mechanical and Aerospace Engineering, Rutgers, The State University of New Jersey, NJ 08854, USA

HIGHLIGHTS

- Experiments revealed relation between heat transfer, ash deposition and corrosion.
- Nusselt number has two rapid drops as the probe wall temperature decreases.
- The first drop occurs when wall temperature is 32–36 °C lower than the ADT.
- Operation of WHRS over the first drop is suggested for coal-fired boilers.

GRAPHICAL ABSTRACT

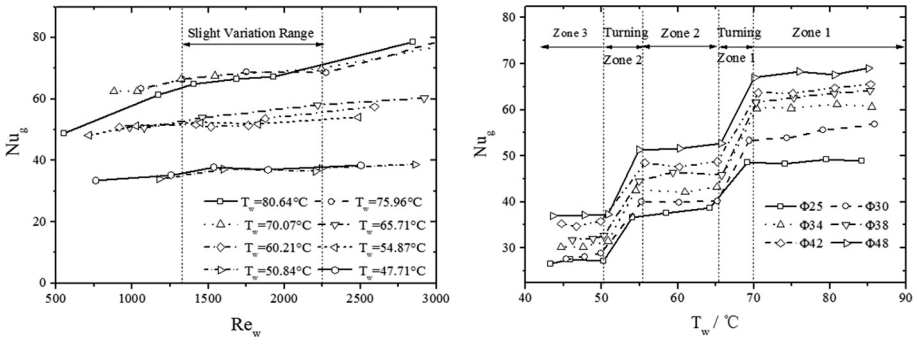

ARTICLE INFO

Article history:
Received 20 October 2016
Revised 26 April 2017
Accepted 27 May 2017
Available online 1 June 2017

Keywords:
Heat transfer
Dew temperature
Ash
Corrosion
Waste heat recovery

ABSTRACT

Waste Heat Recovery Systems (WHRS) have been widely adopted in coal-fired power station boilers, though their heat transfer performance is poor under ultra-low tube temperature circumstances. In this study, we have carried out experiments to reveal heat transfer deterioration and its relation with ash deposition when probe tube temperature varies from 90 °C to ultra-low 40 °C. Results reveal that gas-side Nusselt number has two rapid drops as the probe outer wall temperature decreases. The first drop occurs when the wall temperature is about 32 °C lower than the acid dew temperature, where the deposited ash thickens due to the condensed concentrated sulfuric acid and slight corrosion is observable. The second drop occurs when the wall temperature is about 10 °C greater than the water dew temperature, where the corrosion becomes severe because the concentration of sulfuric acid decreases. For engineering applications, we suggest that the tube outer wall temperature be greater than the first drop temperature to deflate poor heat transfer and surface corrosion.

1. Introduction

Coal is the primary energy source in China. According to BP statistical review of world energy in June 2016 [1], China accounted for 47.7% of world coal production and 50% of world coal consumption in 2015. Underground coal fires after coal mining or during coal mining cause disasters and serious pollution and health problems and recent studies [2,3] have addressed the heat and mass transfer issues to compact underground coal fires. After coal extraction from mines, most of these coals were burned in boilers for various industrial processes. The exhausted flue gas from boilers at about 120–150 °C is a tremendous energy source. Thus, use of waste heat recovery systems (WHRS) has attracted great interest all over the world [4].

* Corresponding authors.
E-mail addresses: shieddie@sdu.edu.cn (Y. Shi), guo@jove.rutgers.edu (Z. Guo).

http://dx.doi.org/10.1016/j.applthermaleng.2017.05.190
1359-4311/

Nomenclature

$A_{ar.zs}$	converted ash content
A_{ar}	ash content of as received base
C_p	specific heat capacity (kJ kg^{-1} K^{-1})
d_ε	characteristic diameter (m)
D_0	outer diameter of the test probe (m)
D_i	outer diameter of inner tube (m)
d_0	inner diameter of outer tube (m)
h	heat transfer coefficient (kW m^{-2} K^{-1})
H_{ar}	hydrogen content of as received base
L	insertion depth (m)
$\dot{M}$	mass flow rate (kg)
Nu	Nusselt number
p	pressure (Pa)
Q	heat transfer rate (kJ)
$Q_{net.ar}$	lower heating value of coal (kJ kg^{-1})
$Q_{gr.ar}$	higher heating value of coal (kJ kg^{-1})
Re	Reynolds number
R	volume percentage
$S_{ar.zs}$	converted sulfur content
S_{ar}	sulfur content of as received base
T	temperature (°C)
V	quantities (N m^3 kg^{-1})
V_{ar}	volatile content of as received base
V_{ad}	coal volatile at air dry base
V_k^0	air quantities (N m^3 kg^{-1})
V_y^0	gas quantities (N m^3 kg^{-1})
W_w	water velocity (m s^{-1})
W_{ar}	total moisture of coal
W_{ad}	coal moisture at air dry base

Greek letters

λ	thermal conductivity coefficient (kW m^{-1} K^{-1})
α_{fh}	coefficient for fly ash
v_w	water kinematic viscosity (m^2 s^{-1})
α	excess air coefficient

Abbreviations

ADT	acid dew temperature
EDS	Energy Dispersive Spectrometer
LPES	low pressure economizer system
ORC	organic Rankine cycles
SEM	Scanning Electron Microscope
WDT	water dew temperature
WHRS	Waste Heat Recovery Systems

Subscripts

g	flue gas
w	wall
out	outlet
in	inlet
y	flue gas

In recent years low-pressure economizer systems (LPES) [5], which heat the condensed water by the waste heat from flue gas, were adopted widely in power station boilers in China. Yang's group has done a lot of researches on waste heat recovery system for flue gas [6–8]. In 2013 they conducted a techno-economic analysis of LPES [6]. In 2014 they proposed an optimized LPES system [7]. In 2015 they proposed a new system that can heat both the condensed water and the air needed to combust [8]. Besides LPES, organic Rankine cycles (ORC) [9,10] have also received interests for their high efficiency and flexibility. Different working media were adopted to waste heat resources with different temperatures [11]. Flue gas cooler is the core equipment for both LPES and ORC systems, which can absorb heat from the exhausted flue gas for different usages. Unfortunately, flue gas cooler suffers from low-temperature corrosion and ash deposition if the flue gas temperature is reduced to acid dew temperature (ADT). Both will deteriorate heat transfer performance and shorten working life of the cooler. Thus, the ultimate temperature after the LPES or ORC system from coal-fired flue gas should remain higher than the ADT, which wastes tremendous energy under ADT.

Is there a limit for WHRS operation in coal-fired flue gas? If it does exit, to what degree can we reduce the flue gas temperature from ADT? These questions are closely related to corrosion and ash deposition under ultra-low temperature flue gas circumstances. There were some studies on low-temperature corrosion and ash deposition [12,13]. Zhao's group in Xi'an Jiatong University has performed some deep researches on coupling effect between low temperature corrosion and ash deposition. In 2013 they established an experimental system to lower the flue gas temperature to about 40 °C to analyze the relationship between ash deposition and corrosion rate [14]. In 2014 they investigated the coupling mechanism between low-temperature corrosion and viscous deposited ashes [15]. In 2016 they conducted a similar research in a biomass-fired circulating fluidized bed boiler instead of coal-fired boiler [16]. Recently, Shi et al. [17] published an experimental study to reveal the mechanisms on low temperature corrosion, but heat transfer performance and its influence were not involved in their study. It is necessary to understand the changing regularity and changing mechanism of heat transfer performance under low-temperature corrosion and ash deposition. This is the innovation and originality in this further study.

Therefore, we concentrate on the influence of low-temperature corrosion and ash deposition on heat transfer performance in this paper. The mechanism of heat transfer deterioration will be revealed, and the minimum wall temperature for long-term and safe operation of WHRS in coal-fired flue gas will be determined. This minimum wall temperature determines ultimately the limitation for waste heat recovery.

2. Description of experiments and methods

2.1. Experimental system

The whole experimental system was installed between the air preheater and the electrostatic precipitator of a 300 MW power unit (see Fig. 1 in Ref. [17]). The technical specifications of the boiler and coal quality were also listed in Table 1 in Ref. [17]. Fig. 1 in the present paper shows the detail of the experimental system, which is composed of three major parts: a constant temperature control system, a test probe, and a measuring system. The probe is a tube heat exchanger and part of it is inserted into the flue gas duct. As shown in Fig. 1, water circulates between the constant temperature control system and the probe. The control system supplies the test probe with constant-temperature water. The water is heated in the test probe and flows back to a tank. The outer wall temperature of the test probe is controlled by the water circulation control system. This temperature represents WHRS tube surface temperature in flue gas duct.

The constant temperature control system contains a water tank, a temperature control device, three valves, a circulating pump, and

Table 1
Structural dimension of test probes.

Item	Symbol	Unit	#1	#2	#3	#4	#5	#6
Total length of the probe	*L*	mm	1200					
Insertion depth	*Lo*	mm	1000					
Insulation length	*Lb*	mm	200					
Total length of inner tube	*Li*	mm	1170					
Diameter of outer tube	*Do*	mm	25	30	34	38	42	48
Diameter of inner tube	*Di*	mm	10	14	16	20	25	30
Thickness of outer tube	δo	mm	2	2.5	3	4	4	4
Thickness of inner tube	δi	mm	0.5	0.5	0.7	1	1	1

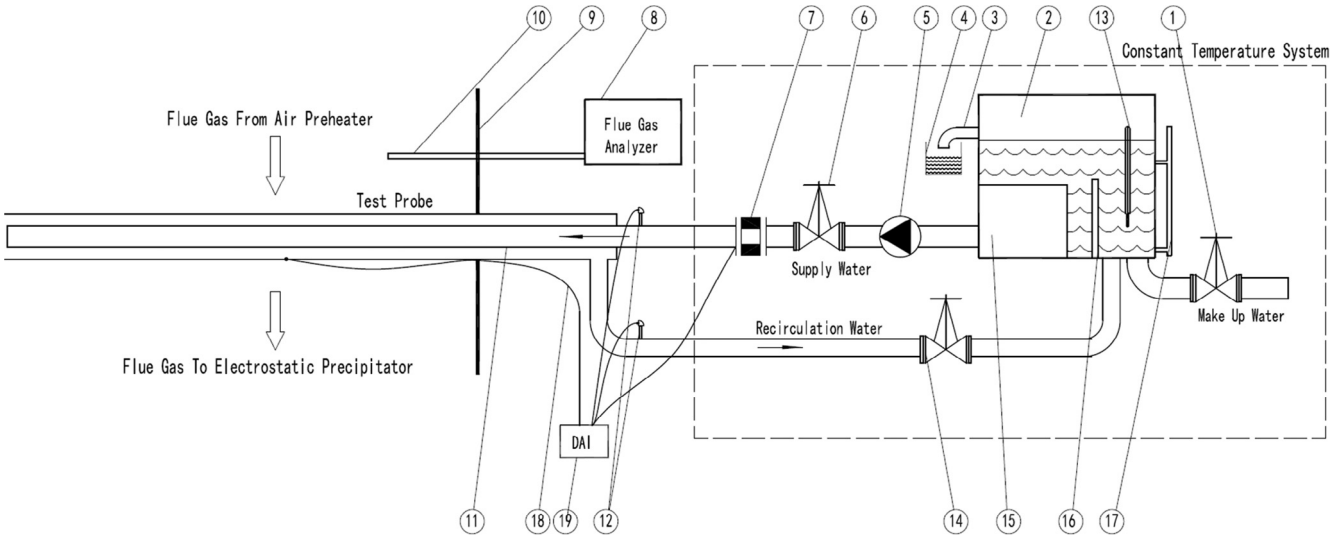

Fig. 1. Experimental system. 1. Makeup water valve; 2. water tank; 3. overflow port; 4. ditch; 5. circulating pump; 6 control valve; 7. flow meter; 8. flue gas analyzer; 9. flue gas duct wall; 10. flue gas analyzer; 11. test probe; 12. water side temperature measuring point; 13. mercurial thermometer; 14. recirculation valve; 15. temperature control device; 16. baffle; 17. water level indicator; 18. wall temperature measuring point; 19. data acquisition instrument.

a flow meter. The water tank can supply sufficient water at set temperature to the test probe. The tank is divided into two zones – a mixing zone and temperature a control zone, by a baffle. There are two orifices located at the bottom of the mixing zone, which are connected to the makeup water and recirculation water, respectively. Here the makeup water at low temperature mixed with the recirculation water at a relative high temperature. The mixed temperature, which is about 5 °C lower than the set value at the temperature control device, can be adjusted by operating the makeup water valve. A mercurial thermometer with accuracy of 0.1 °C was inserted into the mixing zone. This helps the operator to adjust the makeup water valve accurately. The mixed water flows upwards and mixes thoroughly, then over the baffle to the temperature control zone. A temperature control device is installed in this zone, on which the value of temperature can be set. If the water temperature is lower/higher than the set value, the electrical heating rod in the temperature control device will be powered on/off to maintain water temperature at the set value. There also are two orifices in the temperature control zone. One locates at the bottom and connects to the pump. The other is the overflow orifice and locates at the top to prevent water flows out of the tank. The pump supplies water at set temperature through the control valve and flow meter to the test probe.

The structure of the test probe is plotted in Fig. 2. The test probe is of double-layer type and has an inner tube and an outer tube. The two layers are concentric. Thus, the test probe is a coaxial-pipe heat exchanger actually. As shown in Fig. 2, the supplied water initially enters the inner tube and then turns into the outer tube at the opposite end. The test probe was inserted into the gas duct horizontally, only the water inlet and outlet were left outside of the duct. The pressure inside the flue gas duct was negative and ambient air can leak into the gas duct from any tiny clearance, which may affect the experimental result heavily. Thus, the contact area between the duct and the probe was sealed tightly to prevent any air leakage. Hot gas from air preheater flows through the probe crossly. There were 6 different probes used in our tests. The structural data of these probes are listed in Table 1. It is seen from Table 1 that all the data in the length direction are same. It was not easy to keep the inserted probe horizontally when the insertion depth is large. Among different probes, the diameter of outer tube varies from 25 mm to 48 mm, while the diameter of inner tube varies from 10 mm to 30 mm.

The absorbed heat by the cooling water inside the probe equals to the released heat by the hot flue gas to the probe. At the waterside, the inlet and outlet water temperatures of the probe were measured by K-type thermocouples. An electromagnetic flow meter rotameter was used to measure the water flux to the probe. With the water temperatures and flux, the absorbed heat by water can be gained.

The physicochemical property of ash deposited onto the probe surface is determined by the outer wall temperature of the probe. Meanwhile, the heat transfer performance of the probe, ash deposition and accumulation, and corrosion vary with the physicochemical trait of ash. Therefore, the outer wall temperature of the probe is introduced as the characteristic temperature in this work. The outer wall temperature along the inserted probe length may not be constant. It fluctuated within 1 °C at appropriate water flux. So three thermocouples, whose locations are marked in Fig. 2, were set along each probe to measure outer wall temperature and

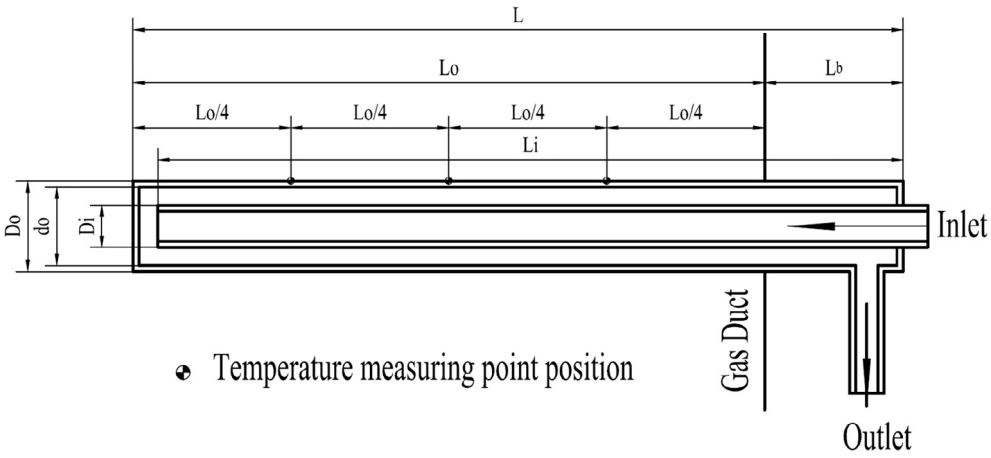

Fig. 2. Structure and dimension of the test probe.

the average reading was used in result analysis. All the measuring signals were sent to a data acquisition device and recorded automatically. Besides, the temperature, oxygen content, and SO_2 concentration of flue gas were measured and recorded by a flue gas analyzer. Monitoring of SO_2 concentration can justify whether coal quality was changed. During the experiment, coal quality and oxygen content should remain unchanged. All the monitored parameters and measuring instruments were listed in Table 3 in Ref. [17].

2.2. Experimental procedure

During the experimental tests, boiler load was remained at 300 MW. The exhaust flue gas temperature is about 131.1 °C. There are measuring holes that allow the test probe to insert into the flue gas duct. In order to reduce the error, the temperature difference between the inlet and outlet is controlled less than 2.5 °C by adjusting the water flux. The difference of three wall temperature points is smaller than 1 °C. Thus, the average value of three values can represent the outer wall temperature of probe. The main experimental procedure is stated as follows:

(1) Turn on the power of the pump and the temperature control device. Set the water temperature to 95 °C. Water circulates between the probe and the tank. Once the inlet temperature of the probe becomes stable and approximately equals to 95 °C, insert the probe into the gas duct. Seal any clearance tightly.
(2) Record the inlet and outlet temperatures of the probe, water flux, and outer wall temperatures by the data acquisition system. Once all the recorded data tend to stable, pull the probe out of the gas duct. Observe ash deposition on the probe and collect ash sample for further analysis by Scanning Electron Microscope (SEM) and Energy Dispersive Spectrometer (EDS).
(3) Clear the deposited ash away from the probe. Repeat the above two steps while the inlet temperature was set from 90 °C to 40 °C, from high to low. The set value was reduced 5 °C each time.

3. Data processing

3.1. Gas-side Nu_g and water-side Re_w

Gas-side Nu_g and water-side Re_w should be calculated to analyze the heat transfer performance according to the experimental data. Gas-side Nu_g is defined as

$$Nu_g = \frac{h_g \times D_0}{\lambda_g} \tag{1}$$

where D_o is the outer diameter of the test probe, λ_g is the flue gas thermal conductivity, h_g is the gas side heat transfer coefficient, which is obtained by

$$h_g = \frac{Q}{\pi D_0 L(T_g - T_w)} \tag{2}$$

where L is the insertion depth, D_o is outer diameter of outer tube, T_g is the flue gas temperature, T_w is the probe outside wall temperature, Q is the heat absorption rate by the cooling water. The heat absorbed can be calculated as

$$Q = C_P \times \dot{M} \times (T_{out} - T_{in}) \tag{3}$$

where $\dot{M}$ is the mass flow rate of the cooling water, T_{out} is the outlet water temperature, T_{in} is the inlet water temperature, and C_p is the specific heat at constant pressure of the water.

Boiler load and coal quality remained stable during the experiment. Volume flux and temperature of the flue gas were stable too. Thus, the gas-side Re_g remained constant during the experiment. The outer wall temperature of the probe depends on the circulation of the cooling water and the probe size under constant flue gas conditions. Water-side Re_w is calculated by

$$Re_W = \frac{w_w \times (d_0 - D_i)}{\upsilon_w} \tag{4}$$

where w_w is the water velocity at the annular flow area between the inner and outer tubes, υ_w is the water kinematic viscosity, and d_e is the characteristic diameter of the annular area, d_o is inner diameter of outer tube, and D_i is outer diameter of inner tube.

3.2. Acid and water dew temperature points

During the experiment, the outer wall temperature T_w of the testing probe drops from about 95 °C to an ultra-low value about 45 °C. It is necessary to know the acid dew temperature (ADT) and water dew temperature (WDT), because ash properties may change when T_w passes through or is close to ADT/WDT. Ash deposition performance and heat transfer performance of the testing probe will be influenced by ash properties.

The acid dew temperature can be calculated as [18]

$$T_{ad} = T_{wd} + \frac{125 \times \sqrt[3]{S_{ar.zs}}}{1.05^{S_{ar.zs}\alpha_{fh}}} \quad (^\circ\mathrm{C}) \tag{5}$$

where T_{wd} is the water dew temperature, α_{fh} is the coefficient for fly ash and equals to 0.9 for pulverized coal boiler, $A_{ar.zs}$ and $S_{ar.zs}$ are converted ash and sulfur contents that can be calculated by

$$A_{ar.zs} = \frac{A_{ar}}{Q_{net.ar}} \times 4190 \quad (\%) \tag{6}$$

$$S_{ar.zs} = \frac{S_{ar}}{Q_{net.ar}} \times 4190 \quad (\%) \tag{7}$$

where $Q_{net.ar}$ is the lower heating value of coal. Recently, we have also introduced the concept of engineering ADT (EADT) and studied the relationship between ash accumulation and EADT [19,20].

T_{wd} equals to the saturation temperature and can be gained by the thermodynamic properties of water and steam once water vapor partial pressure p_{H2O} in the flue gas is known p_{H2O} can be calculated by

$$p_{H2O} = R_{H2O} \times p_{total} \quad (\text{Pa}) \tag{8}$$

where p_{total} is the absolute pressure in the flue gas duct, which is 95,800 Pa. R_{H2O} is the water vapor volume percentage and can be calculated by

$$R_{H2O} = \frac{V_{H2O}}{V_y} \quad (\%) \tag{9}$$

where V_{H2O} and V_y are the total water vapor and flue gas quantities, which can be calculated by

$$V_{H2O} = 0.111H_{ar} + 0.0124W_{ar} + 0.016\alpha V_k^0 \quad (\text{Nm}^3/\text{kg}) \tag{10}$$

$$V_y = V_y^0 + 1.0161(\alpha - 1)V_k^0 \quad (\text{Nm}^3/\text{kg}) \tag{11}$$

where α is the excess air coefficient, $V_k{}^0$ and $V_y{}^0$ are the theoretical air and gas quantities respectively, H_{ar} is hydrogen content of as received base [21]. The calculation equations are below.

$$\alpha = \frac{21}{21 - O_2} \tag{12}$$

where O_2 is the oxygen content of gas at measuring point, and O_2 = 5.8 in the present analysis.

$$V_k^0 = 0.251 \times \frac{Q_{net.ar}}{1000} + 0.278 \quad (\text{Nm}^3/\text{kg}) \tag{13}$$

$$V_y^0 = 0.248 \times \frac{Q_{net.ar}}{1000} + 0.77 \quad (\text{Nm}^3/\text{kg}) \tag{14}$$

$$H_{ar} = 0.07V_{ar} + 0.000165Q_{gr.ar} - 0.0285 \times (100 - W_{ar} - A_{ar}) \tag{15}$$

where V_{ar}, W_{ar}, and A_{ar} are volatile, water and ash contents of coal of as received base respectively, $Q_{gr.ar}$ is gross calorific value of coal. All the items except V_{ar} mentioned above are listed in Table 1. V_{ar} is obtained by

$$V_{ar} = V_{ad} \times \frac{100 - W_{ar}}{100 - W_{ad}} \tag{16}$$

According to the coal quality used in this study, the acid dew temperature and water dew temperature are calculated as 102.3 °C and 39.6 °C, respectively.

4. Results and discussion

The profiles of Nu_g against Re_w at eight different probe outer wall temperatures are plotted in Fig. 3. The inner wall temperature of the probe was sensitive to Re_w; and thus, it was hard to keep the outer wall temperature T_w stable with varying Re_w. So Re_w was controlled such that the flow in the probe was not turbulent. It is seen

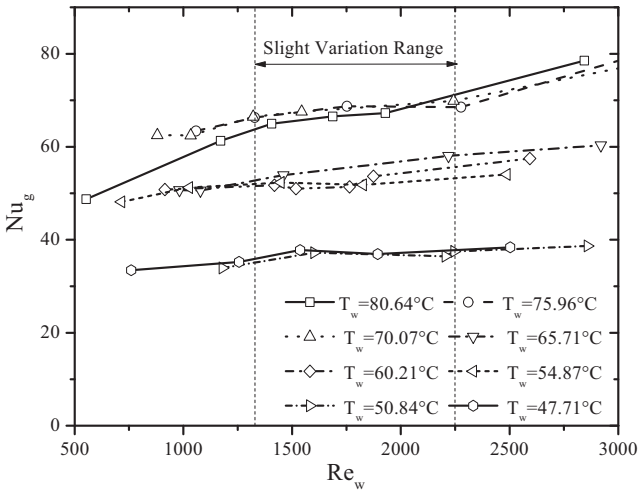

Fig. 3. Nu_g vs Re_w at various wall temperatures for Φ48 test probe.

that water-side Nu_w on the inner wall of the probe increases with Re_w. It is seen that the eight curves can be basically grouped into three typical profiles depending on the wall temperature. There exists a laminar flow Re_w range (1300–2300) in which Nu_g profiles are nearly flat since water-side Nusselt number for laminar fully developed flow region remains constant [22]. Although the flow is laminar in the low Re_w zone (<1300), the difference between the inlet and outlet water temperatures is larger than 2.5 °C because of small water flux. The temperature distribution is greatly uneven along the probe and the determination of the wall temperature with the average value in the three measuring points comes with greater error that affects the value of Nu_g.

Fig. 4 shows Nu_g against the wall temperature within the specific Re_w (1300–2300) range. In this range, both the experimental error, and the impact of cooling water on Nu_g are minimized. It is seen that the larger the outer diameter is, the larger the Nu_g is. This is because the boiler load, flue gas temperature and velocity were stable during the experiment. Thus, gas-side Re_g increases with increasing outer tube diameter. As shown in Fig. 4, the profile of Nu_g vs. T_w is of stepwise style, i.e., Nu_g remains constant within three specific temperature zones with two rapid drops in the two narrow turning zones. Nu_g approximately equals to 68, 52 and 37 for the testing probe of Φ48 when the outer wall temperature T_w is in zone 1 (T_w > 70 °C), zone 2 (54 °C < T_w < 66 °C) and zone 3

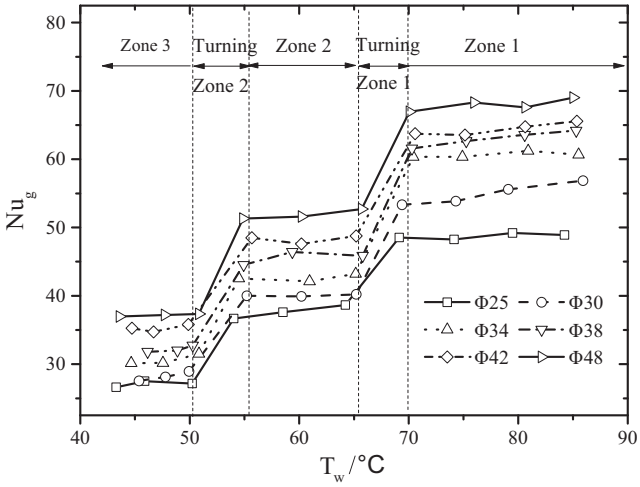

Fig. 4. Nu_g against T_w with Re_w in the range of 1300–2300.

(T_w < 51 °C), respectively. The two turning zones are located in 66 °C < T_w < 70 °C and 51 °C < T_w < 54 °C, respectively.

The stepwise Nu_g distribution is related to the deposited ash properties on the test probe. Ash deposition occurs inevitably on heat transfer surface while firing solid fuel. Photos of ash deposition for the Φ48 testing probe in zone 1 temperature range are shown in Fig. 5. The flue gas velocity in the gas duct at 300 MW was about 15 m/s. There was no ash deposition on the windward side of the probe (Fig. 5a) under such high velocity. On the leeside of the probe, there existed a thin layer of deposited ash because of gas flow vortex (Fig. 5b). Corrosion was not found on the wall after the deposited ash was removed (Fig. 5c). The outer wall temperature of the probe was high enough that little SO_3 condensed in the deposited ash. Thus, the deposited ash was dry, loose and easy to blow off. The fouling resistance coefficient was low and heat transfer performance was very good as Nu_g was higher.

Photos of ash deposition for the Φ48 testing probe with wall temperature in zone 2 lower than 66 °C are shown in Fig. 6. Though the flue gas velocity is unchanged, there is a thick layer of deposited ash on the windward side of the probe (Fig. 6a). The deposited ash on the leeside is humid and a little bit sticky (Fig. 6b). So it is difficult to clean out the deposited ash. Obvious corrosion is observed at the outer wall (Fig. 6c). Compared with Nu_g in zone 1, Nu_g in zone 2 is smaller because of thicker ash layer.

Photos of ash deposition for the Φ48 testing probe in zone 3 temperature range are shown in Fig. 7. The deposited ash on both the windward and leeside side is very humid and accumulates together (Fig. 7a and b). It adheres to the outer wall and was hard to clean. It is so sticky that one can print fingers on it. Severe corrosion is observed after deposited ash is scrapped off (Fig. 7c).

To view small particles clearly in the deposited ash, ash samples were collected for scanning electron microscope (SEM) analysis. SEM photos of ash samples from different zones are shown in Fig. 8. It is seen that the ash particles are loose and small for zone 1 (Fig. 8a). Ash particles separate from each other. Thus, the fouling resistance coefficient is low and Nu_g is high. The adhesion force between particles should be very small. So it is easy to blow off the deposited ash. As the outer wall temperature drops, particle accumulation occurs. The deposited ash becomes denser and larger (Fig. 8b and c). In zone 3 (Fig. 8c), ash particles adhere to each other to form a thick ash layer cling to the probe outer wall. It took great energy to scrape part of the ash layer off. This thick hard layer reduces heat transfer performance and leads to small Nu_g for wall temperature in zone 3.

An energy dispersive spectrometer (EDS) was further employed for elemental analysis of the deposited ash. Ash samples were analyzed as required by *Chinese National Standard - "Microbeam analysis-Quantitative analysis using energy dispersive spectrometry*". Point analysis was adopted because of its higher sensitivity, compared with line and face analysis. The relative errors for EDS analysis depend on the element weight percentage and are shown in Table 2.

EDS spectra of ash samples in different temperature zones were displayed and discussed in Ref. [17]. From Fig. 3(b) in Ref. [17] it is known that the major elements in the ash sample in zone 1 were O, Si, Al, and Ca. The chemical compound should be SiO_2, Al_2O_3, and Wollastonite, which are major incombustible matter of coal. For the ash sample from zone 2 (see Fig. 5b in Ref. [17]), the weight percentage for S and Fe are 0.16% and 1.55%, respectively, whose chemical compound should be $FeSO_4$. This is why there exists slight corrosion on the probe in zone 2 (see Fig. 9b in Ref. [17]). While for ash sample from zone 3, the weight percentage for S and Fe rise to 5.98% and 37.54%, respectively, which explains severe corrosion on the probe in zone 3 (Fig. 7c in the present paper).

Water vapor, SOx, and ash are important components in flue gas. SOx and water vapor can react into H_2SO_4 vapor. When the outer wall temperature is high enough, H_2SO_4 vapor adjacent to the outer wall is of gaseous state. H_2SO_4 vapor begins to condensate at acid dew temperature (ADT). ADT is a function of the partial pressure of H_2SO_4 vapor. Generally, local ADT drops with decreasing partial pressure of H_2SO_4 vapor [23]. When T_w is slightly lower

(a) windward side view of the testing probe

(b) leeside view of the testing probe

(c) leeside view with deposited ash scraped off

Fig. 5. Photos of the Φ48 test probe in zone 1.

(a) windward side view of the testing probe

(b) leeside view of the testing probe

(c) leeside view with deposited ash scraped off

Fig. 6. Photos of the Φ48 test probe in zone 2.

(a) windward side view of the testing probe

(b) leeside view of the testing probe

(c) leeside view with deposited ash scraped off

Fig. 7. Photos of the Φ48 test probe in zone 3.

than the local ADT, the partial pressure of H_2SO_4 vapor decreases because part of the H_2SO_4 vapor condensates into liquid acid, leading to a decrease of the local ADT. Thus, the condensation may not continue and the condensed sulfuric acid is so rare that it has little influence on ash property. The deposited ash particles remains dry and separate from each other, just like that with temperature over ADT. Therefore, no accumulation and corrosion occurred on the probe, no large particles were detected in the SEM analysis, no Fe and S were found in EDS photos, and the deposited ash was easy

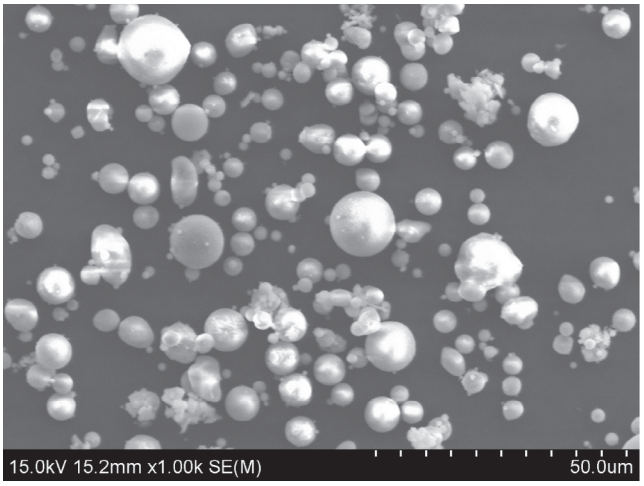

(a) Zone 1

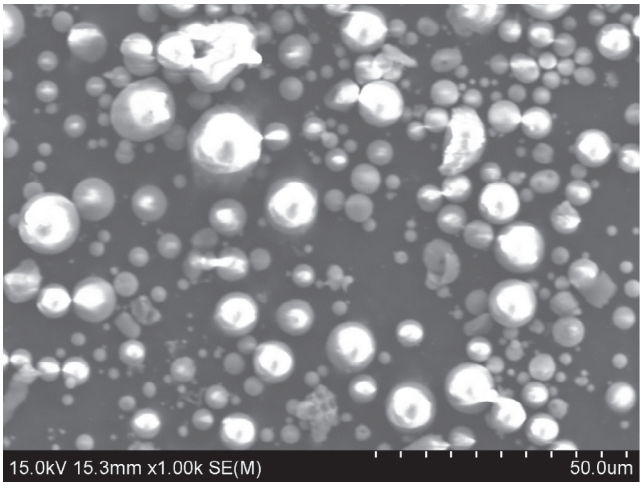

(b) Zone 2

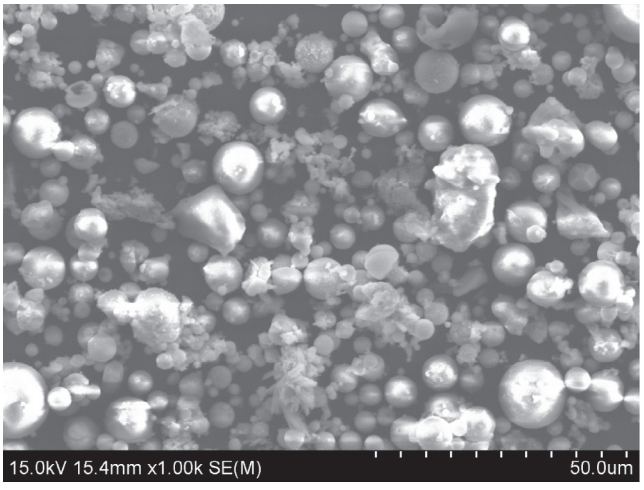

(c) Zone 3

Fig. 8. SEM photos of the ash samples in different zones.

to blow off. The component of the deposited ash is just incombustible matter of coal. All the phenomena mentioned above are characteristics of zone 1.

With the T_w drops farther from ADT, the H_2SO_4 vapor condensation produces more concentrated liquid acid. The deposited ash absorbs the liquid acid and increase the adhesion force between particles. When T_w goes down to a certain temperature range, the adhesion force becomes strong enough for particles to accumulate when collision happens. With accumulation goes on, the probe surface will inevitably change from that partly covered by separated dry particles to that fully covered by accumulated humid particles. The temperature range that ash particles on the probe surface begin to accumulate is the turning zone 1 (66–70 °C) shown in Fig. 4. The accumulated deposited ash is too sticky to clear off and the fouling thermal resistance increases. Thus, gas-side Nu_g has a sudden drop at turning temperature zone 1. Besides, chemical reaction between liquid acid, incombustible matter of coal and heat transfer surface occurs to produce $FeSO_4$; but the reaction is slow because of concentrated acid. Fe and S can be detected by EDS although their contents are rare. Those are characteristics of zone 2. In our experiments conducted, the turning temperature is about 32 °C lower than the ADT.

Table 2
Relative errors for EDS.

Relative error	Element weight percentage
<5%	>20%
<10%	3–20%
<30%	1–3%
<50%	0.5–1%

As T_w goes down from zone 2, it is much lower than the local ADT, but higher than the WDT. Massive H_2SO_4 vapor condensates to produce more and more concentrated acid. Oxygen content in the concentrated sulfuric acid is relatively high. Thus, passivation occurs on metal surface of tube bundle. Corrosion rate between metal and acid is low. But the concentrated sulfuric acid has a strong ability to absorb water vapor from flue gas. It actually acts as desiccant. With absorption goes on, water content in the deposited ash becomes larger and larger. When T_w goes down to a certain temperature range, sufficient water vapor is absorbed by the concentrated acid, and the concentrated acid turns into dilute acid with certain oxygen content [24]. The protection film on metal surface caused by passivation vanishes and corrosion accelerates. More and more $FeSO_4$ appears. It is loose and enlarges the thermal resistance in a short time. The sudden drop of heat transfer performance occurs within turning zone 2, which is about 10 °C higher than the WDT.

In practical point of view, as long as the outer wall temperature is in zone 1, the deposited ash will be thin and easy to blow off. It does not impact heat transfer performance and introduces no corrosion on the tube heat transfer surface. In a limit case, the exhausted flue gas temperature can be reduced to the sum of the minimum value in zone 1 and a reasonable heat transfer temperature difference between tube wall and flue gas. Thus, the maximum limit for waste heat recovery can be determined.

5. Conclusions

Experimental studies have been conducted to investigate the heat transfer deterioration, ash deposition, and corrosion for tube heat transfer surface under ultra-low tube wall temperature circumstance for WHRS in boilers. The experimental result reveals that the gas-side Nu_g experiences two rapid drops with decreasing tube outer wall temperature.

When T_w was higher than 70 °C, which was about 32 °C lower than ADT, there was no obvious ash deposition on the testing probe. Nu_g was high and no corrosion was observed. As T_w drops below 66 °C but above 54 °C ash deposits because of the condensed concentrated sulfuric acid and the deposition becomes thicker and

sticker, which reduces heat transfer performance to a mediate Nu_g and accompanies with slight corrosion. As T_w further drops below 51 °C, $FeSO_4$ content has a sharp increase because of increased corrosion, resulting in a further reduction in Nu_g and severe corrosion. The present experiments observed two turning zones – the first one occurs when the wall temperature is about 32–36 °C lower than the ADT, and the second one is about 10 °C higher than the WDT.

To operate and design WHRS in practical boilers, it is critical that the tube outer wall temperature should be higher than the first turning temperature zone so that the heat transfer performance of the heat transfer tube bundle is not affected by ash deposition and sulfuric acid corrosion. The limit for waste heat recovery can be determined when the exhausted flue gas temperature is reduced to the sum of the minimum value in zone 1 and a reasonable heat transfer temperature difference between tube wall and flue gas.

Acknowledgment

The authors acknowledge the financial support provided by the Chinese National Development and Reform Commission on Low-carbon Technological Innovation and Industrial Demonstration Project on Power Industry ([2003] 1819).

References

[1] BP statistical review of world energy 2016, Viewed: August, 2016.
[2] Y. Wang, G. Shi, Z. Guo, Heat transfer and thermodynamic processes in coal-bearing strata under the spontaneous combustion condition, Numer. Heat Trans., Part A: Appl. 71 (2017) 1–16.
[3] M. Liu, G. Shi, Z. Guo, Y. Wang, 3-D simulation of gases transport under condition of inert gas injection into goaf, Heat Mass Trans. 52 (2016) 2723–2734.
[4] G. Oluleye, M. Jobson, R. Smith, S.J. Perry, Evaluating the potential of process sites for waste heat recovery, Appl. Energy 161 (2016) 627–646.
[5] C. Wang, B. He, L. Yan, X. Pei, S. Chen, Thermodynamic analysis of a low-pressure economizer based waste heat recovery system for a coal-fired power plant, Energy 65 (2014) 80–90.
[6] G. Xu, S. Huang, Y. Yang, Y. Wu, K. Zhang, C. Xu, Techno-economic analysis and optimization of the heat recovery of utility boiler flue gas, Appl. Energy 112 (2013) 907–917.
[7] G. Xu, C. Xu, Y. Yang, Y. Fang, Y. Li, X. Song, A novel flue gas waste heat recovery system for coal-fired ultra-supercritical power plants, Appl. Therm. Eng. 67 (2014) 240–249.
[8] Y. Yang, C. Xu, G. Xu, Y. Han, Y. Fang, D. Zhang, A new conceptual cold-end design of boilers for coal-fired power plants with waste heat recovery, Energy Convers. Manage. 89 (2015) 137–146.
[9] G. Kosmadakis, D. Manolakos, G. Papadakis, Experimental investigation of a low-temperature organic Rankine cycle (ORC) engine under variable heat input operating at both subcritical and supercritical conditions, Appl. Therm. Eng. 92 (2016) 1–7.
[10] H. Łukowicz, A. Kochaniewicz, Analysis of the use of waste heat obtained from coal-fired units in Organic Rankine Cycles and for brown coal drying, Energy 45 (2012) 203–212.
[11] M. Li, B. Zhao, Analytical thermal efficiency of medium-low temperature organic Rankine cycles derived from entropy-generation analysis, Energy 106 (2016) 121–130.
[12] A. Kranzmann, T. Neddemeyer, A.S. Ruhl, D. Huenert, D. Bettge, G. Oder, R.S. Neumann, The challenge in understanding the corrosion mechanisms under oxyfuel combustion conditions, Int. J. Greenhouse Gas Control 5 (2011) S168–S178.
[13] Z. Tang, X.P. Chen, D.Y. Liu, Y.M. Zhuang, M.H. Ye, H.C. Sheng, S.J. Xu, Experimental investigation of ash deposits on convection heating surfaces of a circulating fluidized bed municipal solid waste incinerator, J. Environ. Sci. 48 (2016) 169–178.
[14] Y.G. Wang, Q.X. Zhao, Z.X. Zhang, Mechanism research on coupling effect between dew point corrosion and ash deposition, Appl. Therm. Eng. 54 (2013) 102–110.
[15] Z.Y. Liang, Q.X. Zhao, Y.G. Wang, Y.X. Li, Z.C. Zhang, Coupling mechanism of dew point corrosion and viscous ash deposits, Mater. Corros. 65 (2014) 797–802.
[16] Y. Wang, H. Ma, Z. Liang, H. Chen, Q. Zhao, X. Jin, Experimental study on dew point corrosion characteristics of the heating surface in a 65 t/h biomass-fired circulating fluidized bed boiler, Appl. Therm. Eng. 96 (2016) 76–82.
[17] Z.M. Li, F.Z. Sun, Y.T. Shi, F. Li, L. Ma, Experimental study and mechanism analysis on low temperature corrosion of coal fired boiler heating surface, Appl. Therm. Eng. 80 (2015) 355–361.
[18] D.F. Che, Boilers-Theory, Design and Operation, Xi'an Jiaotong University Press, 2008.
[19] Y. Shi, X. Wang, D. Chu, F. Sun, Z. Guo, An experimental study of ash accumulation in flue gas, Adv. Powder Technol. 27 (2016) 1473–1480.
[20] Y. Shi, Z. Ma, D. Chu, X. Wang, F. Sun, Z. Guo, An experimental study of ash particles adhesion force in flue gas, Adv. Powder Technol. 28 (2017) 1435–1442, http://dx.doi.org/10.1016/j.apt.2017.03.010.
[21] V. Meer, G. Wesselink, Determination of gross calorific value by the calorimetric bomb method: statistical evaluation of the collaborative study ISO / TC 34 / SC 10 animal feedings stuffs, Indian J. Med. Res. 58 (1985) (1985) 1510–1522.
[22] W. Rohlfs, J.H. Lienhard, Entrance length effects on Graetz number scaling in laminar duct flows with periodic obstructions: Transport number correlations for spacer-filled membrane channel flows, Int. J. Heat Mass Transf. 97 (2016) 842–852.
[23] P. Muller, Contribution to the problem of the action of sulfuric acid on the dew point temperature of flue gases, Chem. Eng. Tech. 31 (1959) 345–350.
[24] Z. Panossian, N.L.d. Almeida, R.M.F.d. Sousa, G.d.S. Pimenta, L.B.S. Marques, Corrosion of carbon steel pipes and tanks by concentrated sulfuric acid: A review, Corros. Sci. 58 (2012) 1–11.